Variational multiscale large-eddy simulations of the flow past a circular cylinder : Reynolds number effects

Stephen Wornom[a], Hilde Ouvrard[b], Maria Vittoria Salvetti[c], Bruno Koobus[b], Alain Dervieux[a]

[a]*INRIA, 2004 Route des lucioles, BP 93, 06902 Sophia Antipolis (France)*
[b]*Institut de Mathématiques et de Modélisation de Montpellier, Université Montpellier 2, Case Courrier 051, Place Eugène Bataillon, 34095 Montpellier (France)*
[c]*Dipartimento di Ingegneria Aerospaziale, Università di Pisa, Via G. Caruso 8, 56122 Pisa (Italy)*

Abstract

Variational-multiscale large-eddy simulations (VMS-LES) of the flow around a circular cylinder are carried out at different Reynolds numbers in the sub-critical regime, viz. Re=3900, 10000 and 20000, based on the cylinder diameter. A mixed finite-element/finite-volume discretization on unstructured grids is used. The separation between the largest and the smallest resolved scales is obtained through a variational projection operator and finite-volume cell agglomeration. The WALE subgrid scale model is used to account for the effects of the unresolved scales; in the VMS approach, it is only added to the smallest resolved ones. The capability of this methodology to accurately predict the aerodynamic forces acting on the cylinder and in capturing the flow features are evaluated for the different Reynolds numbers considered. The sensitivity of the results to different simulation parameters, viz. agglomeration level and numerical viscosity, is also investigated at Re=20000.

Keywords: Variational multiscale LES, circular cylinder, unstructured grids

1. Introduction

Today large-eddy simulations (LES) are increasingly used for engineering and industrial applications, at least for those flows for which the RANS approach encounters difficulties in giving accurate predictions. Paradigmatic examples of such flows are bluff-body wakes.

The present work is part of a research activity aimed at developing and validating methodologies for the application of LES to flows of industrial or engineering interest, *i.e.* characterized by complex realistic geometries and a dynamics involving a wide range of time and space scales. The role and interaction of closure modeling and numerical discretization (grid resolution and schemes) in LES is much different than in RANS and, thus, for application of LES in an industrial context, peculiar issues arise and ad-hoc methodologies and strategies need to be developed and validated (see e.g. [1, 2, 3] for recent reviews and discussions). Our strategy is based on the following key ingredients : (i) unstructured grids, (ii) a second-order accurate numerical scheme stabilized by a numerical viscosity proportional to high-order space derivatives, and thus acting on a narrow band of smallest resolved scales, and tuned by an ad-hoc parameter, (iii) Variational Multi-Scale (VMS) formulation combined with eddy-viscosity subgrid scale (SGS) models. The motivations of these choices are extensively discussed in our previous publications [4, 5, 6] and are not reported here for the sake of brevity. We would just like to recall that a key feature of VMS-LES [7] is that the SGS model is only added to the smallest resolved scales. This is aimed at

reducing the excessive dissipation introduced by non-dynamic eddy-viscosity SGS models also on the large scales and this has been shown to generally improve the behavior of such models, such as for instance for the Smagorinsky model in boundary layers [8]. Clearly, the VMS approach is a possible choice among several strategies proposed in the literature to improve the behavior of eddy-viscosity SGS models, such as, for instance, the dynamic procedure [9] ([10, 11] for anisotropic grids) or the combination with scale-similarity terms [12]. The VMS approach is particularly attractive for variational numerical methods and unstructured grids, because it is easily incorporated in such formulations [8, 13] and the additional computational costs with respect to classical LES are very low, while other approaches may bring rather large additional complexity and computational costs (see e.g. [4]).

In a previous work [6], we applied the VMS methodology, together with three different eddy-viscosity SGS models, to the flow around a circular cylinder at a Reynolds number of 3900; the results were appraised against experiments and LES simulations in the literature and compared with those obtained with the same models and simulation parameters in classical LES. In the present paper, a further contribution to the appraisal of the VMS methodology is given by the application to the same flow configuration when the Reynolds number is increased from 3900 to 20000.

This interval lies in the intermediate subcritical regime (see e.g. [14]). The lower part of this interval has been the subject of many experimental studies, summarized e.g. in [15]. In the Achenbach drag-vs-Reynolds curve [16, 18], the interval 3900-20000 corresponds to a section of slow but continuous increment of drag. The drag is reaching a minimum around Re=2000-3000 and

increases slowly to a quasi-plateau attained around Reynolds 20000. Furthermore, noticeable variations of lift fluctuations and of the mean base pressure have been observed when the Reynolds number is varied in this regime, while the Strouhal number is only marginally decreasing (see the discussion and the references in [15] and [17]). The changes in aerodynamic forces are certainly related to the instability of the separating shear-layers, which moves upstream with increasing Reynolds number, leading to a significant reduction of the formation length of the Karman vortices, firstly observed in [19]. Furthermore, a crucial phenomenon occurring in this Reynolds number range is the onset and the amplification of the Kelvin-Helmholtz (KH) instability in the free shear layer formed from the surface of cylinder, producing small-scale vortices (see [20], [21]). For reviews of the literature on shear-layer instability/transition in the cylinder near wake, the reader is referred to [15, 22, 23, 24]. Several observations do not detect KH small vortices at Re=5000 (see for example [25]) but detect them at Re=10000. In contrast to this, KH vortices are observed in DNS at Re=3900 by Dong et al., [24]. These differences may be due to the fact that in the subcritical regime, corresponding more or less to a Reynolds number ranging from 1000 to 5000, the KH vortical structures appear in avery intermittent way and, therefore, it is difficult to observe them on instantaneous flow visualizations. However, all the previous studies agree that, as the Reynolds number increases, the high-frequency fluctuations in the velocity signals, caused by the KH vortices become more and more important and eventually dominate the fluctuations caused by the Karman vortex shedding. The ratio between the shear-layer frequency and the vortex shedding frequency also increases as a power of

Reynolds number, see [22, 23].

From a more general viewpoint, many measurements are available for this interval of Reynolds number. For the interval 3900-4020, see for example [26, 27, 28, 29, 24]. Also, several experiments have been carried out for intermediate Reynolds number. Let us mention [17] for Reynolds number 8000. For a Reynolds number of 20000, results are reported in [30] and [31]. Moreover, measures for Reynolds numbers of 16000 and 24000 are documented in [33].

The aim of the present work is, thus, to investigate whether the methodology previously described is able to predict, on an unstructured grid as those often used in industrial applications, the variation of aerodynamic forces and base pressure and to capture the phenomena briefly recalled above, which characterize the Reynolds number range under investigation. As previously said, the study is carried out for the VMS-LES formulation and, among the SGS models investigated in [6], the Wall-Adapting Local Eddy-viscosity (WALE) SGS model proposed in [34] is used herein. Due to its design feature, the WALE model exhibits the correct near-wall behavior while being a simple eddy-viscosity model. As noted earlier, this feature is not necessary if we combine the WALE model with the VMS approach. However, in our study [6] conducted at Reynolds number 3900, we observed that for the WALE model the VMS approach was particularly effective in reducing the excessive dissipation of WALE in classical LES formulation and improved the quality of the predictions. This is in agreement with the findings of [35], in which a high-pass filtered multiscale version of the WALE model was proposed in order to reduce its dissipation for vortical flows. Finally, to our knowledge, the

application of the VMS-LES approach and of the WALE SGS model to this type of flow is not documented in the literature, except in [6]. In the present paper, the results obtained at Reynolds numbers equal to 3900, 10000 and 20000 are presented.

The corresponding flow at Reynolds number 3900 has been well studied, see, e.g., the LES computations in [36, 6, 27, 37] and the DNS studies in [24]. The intermediate Reynolds number of 8000 has been computed by LES in [38]. For Reynolds number 10000, we refer to DNS simulations in [24]. The same flow at Reynolds number 20000 has been computed in [32] through LES with different SGS models, and in [39] with a TVD numerical method without a subgrid scale model. These studies are used for comparison, together with the experimental data previously cited. We first compare the results obtained at the different Reynolds numbers without changing any simulation parameter; in particular, the same grid, having approximately 1.8×10^6 nodes is used in all the simulations. Finally, in analogy with the investigation carried out at Re=3900 in [6], the sensitivity of the results to different simulation parameters, viz. agglomeration level and numerical viscosity, is investigated at Re=20000.

2. Methodology

A more complete description of the methodology can be found in [5] and in [6]; we just briefly recall its main features.

The filtered Navier-Stokes equations for compressible flows and in conservative form are considered. The WALE SGS eddy-viscosity model [34] is used to close the equations. The governing equations are discretized in space

through a mixed finite-element/finite-volume method applicable to unstructured grids. The resulting scheme is second-order accurate and is stabilized through a very low numerical diffusion built with a sixth-order spatial derivative, weighted by the 5th power of local mesh size and by a tunable coefficient γ. The impact of this stabilizing term has been evaluated as very low (see e.g. [5] and [6]). A key ingredient is the VMS formulation. In short, a splitting is introduced between the large resolved scales (LRS), *i.e.* those resolved on a virtual coarser grid (roughly of size $2\Delta x$, Δx being the local grid resolution) and the small resolved ones (SRS, of size Δx). The scale separation is obtained through a projector operator in the LRS space, which is based on spatial average on macro-cells, obtained through agglomeration of the finite-volume cells associated to the used grid [13]. The SGS WALE model is then restricted to the SRS, the larger ones being influenced by the introduced SGS viscosity only through the coupling with the SRS. Finally, we adopt herein the so called small-small formulation, *i.e.* the SGS term is computed as a function of the SRS only.

3. Test-case and numerical set-up

Simulations are carried out for the flow around a circular cylinder, at Reynolds numbers, based on the cylinder diameter, D, and the freestream velocity, equal to 3900, 10000 and 20000 respectively. The computational domain is such that $-10 \leq x/D \leq 25$, $-20 \leq y/D \leq 20$ and $-\pi/2 \leq z/D \leq \pi/2$, where x, y and z denote the streamwise, transverse and spanwise directions respectively, the cylinder center being located at $x = y = 0$. No-slip conditions are applied on the cylinder surface. In the spanwise direction,

periodic boundary conditions are imposed, while characteristic based conditions are used at the inflow and outflow as well as on the lateral boundaries ($y/D = \pm 20$). The freestream Mach number is set equal to 0.1 in order to make a sensible comparison with incompressible simulations in the literature. Preconditioning is used to deal with the low Mach number regime [6]. As discussed in the Introduction, we decided first to compare the results obtained in simulations carried out at different Reynolds numbers using the same parameters and computational conditions. Thus, the same grid is used, namely an unstructured tetrahedral grid of approximately 1.8×10^6 nodes (GR1). The averaged distance of the nearest point to the cylinder boundary is 0.001D, and 100 nodes are present in the spanwise direction near the cylinder, with an approximately uniform distribution. This grid has been designed to have a reasonable resolution at all the considered cases, without ad-hoc adaptation, as often is the case in engineering applications. Moreover, as for modeling, the free parameter in the WALE SGS model is set equal to 0.5, as suggested in [34], the filter width is defined as the third root of the volume of the grid elements, as in [6], and the macro-cells used in the VMS procedure are obtained from the finite-volume cells associated to the computational grid by means of one level of agglomeration. Finally, as for numerics, the parameter controlling the amount of numerical viscosity is set to 0.3 (see also [6]).

As for computational costs, for 30 vortex shedding cycles and with 64 cores, the CPU time is approximately 100 hours over a SGI Altix ICE computer.

4. Results at different Reynolds numbers

Let us consider, first, the main bulk flow parameters. For all the simulations, statistics are computed by averaging in the spanwise homogeneous direction and in time for at least 30 vortex-shedding cycles, after having discarded the initial transient after the impulsive start-up. The bulk flow parameters for Re=3900 are presented in Tab. 1. They are compared with the LES calculations of [27, 36, 37] and the measurements of [24, 26, 27]. We also report the results of the simulations in [6], carried out with the same modeling and parameters, but on two different grids having 2.9×10^5 and 1.46×10^6(see [6] for more details). The bulk flow parameters for Re=10000 are presented in Tab. 2 and compared with the direct numerical simulations of [24] and the measurements of [28, 17, 40, 41]. Finally, the bulk flow parameters for Re=20000 are presented in Tab. 3. They are compared with the LES calculations of [39, 32] and the measurements of [17, 33, 30, 31].

As for the Strouhal number associated to vortex shedding, St, Tabs. 1-3 show that the slight decrease with increasing Reynolds number, observed in the experiments, seems to be correctly captured in the VMS-LES simulations. In [17] a review of the fluctuating lift acting on circular infinitely-long cylinders at Reynolds numbers ranging from 47 to 2×10^5 was carried out and empirical functions were proposed for the Reynolds number dependence of St and of the r.m.s. of the lift coefficient. Fig. 1(a) shows that the results of the present simulations, also reported in Tabs. 1-3, agree well with the proposed empirical functions.

Another feature which seems to be correctly reproduced in the present VMS-LES simulations is the fact that the formation length of the Karman

vortices decreases as the Reynolds number increases, as observed in the literature for the considered Reynolds number range (e.g. [19]). This is qualitatively shown by the instantaneous vorticity isocontours obtained at different Reynolds numbers and shown in Figs. 2-4. More quantitatively, this is also indicated by the decrease of the mean recirculation bubble length, l_r with increasing Reynolds number. Indeed, the smaller is the formation length of the Karman vortices, the smaller is the mean recirculation bubble length. This trend is captured in the present simulations and, for all the considered Reynolds numbers, the obtained values are in very good agreement with the available experimental and/or numerical data in the literature.

As a consequence of the reduced length of formation of the Karman vortices, the absolute value of the mean base pressure coefficient, and, consequently, the mean drag coefficient increase with the Reynolds number, as can be seen in Tabs. 1-3. Furthermore, the amplitude of the oscillations in time of the lift coefficient also increase with the Reynolds number. All these trends are again captured in the present simulations. As for the r.m.s. of the lift coefficient, the quantitative agreement with the available numerical and experimental data in the literature is good for all the considered Reynolds numbers. Fig. 1(b) shows a comparison of the present results with the empirical functions proposed in [17]. An overestimation of the r.m.s. of the lift coefficient is observed at $Re = 10000$ and $Re = 20000$; however, a significant scatter of the experimental data reviewed in [17] is observed in this range of Reynolds numbers and the present results seem to be in good agreement with the experimental data giving the highest values of C_{Lrms} (see Fig. 2 in [17]).

At Re=3900, the mean pressure drag and the base pressure are well predicted (Tab. 1), while they are both slightly overestimated at Re=10000, the errors being of 2.5% for $\overline{C_d}$ and of 3.6% for $\overline{Cp_b}$. Note that there is close agreement with the range of the predictions obtained in the DNS of [24] for different grid resolutions. At Re=20000 the overprediction of the mean drag coefficient is slightly larger than at Re=10000 (5.8% with respect to the highest limit of the experimental range), while the value of the base pressure is rather good.

The mean drag prediction is clearly related to that of the pressure distribution over the cylinder. Figs. 5-7 show the mean pressure coefficient distribution at the cylinder obtained at the different Reynolds numbers, compared to reference experimental data [29, 24, 30]. Although the overall agreement is good, at all the considered Reynolds numbers there is a slight overestimation of the mean C_p at the stagnation point. This is due to the fact that a compressible flow solver is used; even if the Mach number is low (M=0.1) and ad-hoc preconditioning is used, small compressibility effects are present at the stagnation point. The same slight overestimation can be observed in the results reported in [6]. The agreement in the separated wake is excellent at $Re = 3900$, while some discrepancies can be observed at $Re = 10000$ and $Re = 20000$, and this explains the small errors in the prediction of the mean drag coefficient. If we consider, as often done in the literature, the point at which the slope of the mean C_p curve changes (after the minimum) as an indicator of the location of boundary-layer separation, this seems to be correctly captured in the present simulations for all the considered Reynolds number. For the present simulations, the separation point has also been de-

tected from the averaged velocity field and the results are reported in Tabs. 1-3; it slightly moves upstream as the Reynolds number increases, but there are not significant variations.

As previously discussed in the Introduction, another characteristic feature in the considered Reynolds number range is the onset of the KH instability of the detaching shear layers, leading to the formation of small-scale vortices. Looking at the instantaneous vorticity iso-contours at Re=3900 in Fig. 2, there is no evidence of small-scale vortical structures. This is consistent with the vorticity visualizations in [25] (Re=5000) and in [24] (Re=4000). In [24] these structures are identified at Re=4000 by instantaneous velocity vectors and spectral analysis of velocity time signals recorded in the shear layers. The lack of KH vortical structures in our vorticity snapshots at Re=3900 may also be due to the intermittency of these structures at this Reynolds number value, which makes difficult to detect them on instantaneous flow visualizations. More surprisingly, the small-scale structures are not clearly visible even at Re=10000 and Re=20000 (Figs. 3 and 4a). In order to investigate whether this is due to a lack of grid resolution, we have transfered our established (vortex shedding) solution on a 3.8 million nodes grid, obtained by local division of the tetrahedra located in the boundary layer and in the shear layers, and a few shedding cycles have been simulated on this finer grid. The instantaneous iso-contours of vorticity obtained in this simulation are shown in Fig. 4b and the small-scale KH vortices are clearly detectable. This indicates that for an accurate description of the K-H shear-layer instability a finer grid resolution is probably needed, as it could be expected since these instabilities are associated with frequency which significantly increase

with the Reynolds number [24, 15, 23] and thus they are related to progressively smaller scales. Note, however, that although these structures are not well resolved in the present simulations, their effects on the bulk quantities of practical interest, such as the aerodynamic loads on the cylinder, are satisfactorily reproduced.

5. Parameter sensitivity analysis at Re=20000

Finally, an analysis of the sensitivity to different simulation parameters is carried out at Re=20000. The effect of numerical diffusion is first investigated by varying the value of the parameter γ, which directly multiplies the upwind part of the numerical convective fluxes [5, 6]. In all the previously analyzed simulations this parameter was set to 0.3. We consider now a simulation carried out at Re=20000 with $\gamma = 0.2$ and Tab. 4 show the percent variation of the bulk parameters obtained in this simulation with respect to those in Tab. 3. Note that the simulation in Tab. 4 and the one in Tab. 3 only differ for the value of γ, all the remaining parameters being unchanged. It can be seen that the sensitivity of the predictions to γ, *i.e.* the parameter controlling the numerical diffusion, is very low. This is in agreement with the findings at Re=3900 and of our previous works [4, 5, 6] and confirms that the numerical diffusion introduced by the present numerical scheme does not play a predominant role, also when used in the VMS-LES approach, in which the SGS viscosity is lower than in classical LES and is applied to a limited range of scales. It is also confirmed that a fine tuning of the parameter γ is not needed in order to limit the spurious effects of the numerical diffusion.

The sensitivity to the level of agglomeration, which controls the range of

the scales at which the SGS model is added, has also been investigated by carrying out a simulation in which the LRS space is defined by the projection onto macrocells obtained through two agglomeration steps. This means that the large resolved scales in the VMS-LES WALE with two levels of agglomeration in Tab. 4 are roughly those having a dimension three times larger than the local grid resolution. Thus, the SGS model is acting on a wider range of scales than in all the previous VMS-LES simulations. Nonetheless, the sensitivity to this parameter is also low, as shown in Tab. 4.

6. Concluding Remarks

Variational-multiscale large-eddy simulations of the flow around a circular cylinder carried out at different Reynolds numbers in the subcritical regime, viz. Re=3900, 10000 and 20000, have been presented and analyzed. The key ingredients of the used numerics and modeling are : unstructured grids, a second-order accurate numerical scheme stabilized by a tunable numerical diffusion proportional to high-order space derivatives and the VMS formulation combined with the WALE subgrid model. The simulations are carried out at different Reynolds numbers without any change in the parameters. This is useful to investigate the capabilities of the used methodology to capture Reynolds number effects in the subcritical regime without any ad-hoc adjustement. For all the main bulk flow quantities, viz. the vortex-shedding Strouhal number, formation length of Karman vortices, mean recirculation bubble length, aerodynamic loads and pressure distribution, the trends observed in the literature for Reynolds numbers in the considered range are correctly reproduced in the present simulations. The quantitative agreement

with available experimental and numerical data is generally good. Small discrepancies observed at Re=10000 and 20000 can be explained by the lack of resolution, which obviously becomes coarser as the Reynolds number increases. In particular, a finer grid resolution is needed for an accurate description of the KH small-scale vortices, which are associated with frequencies which are significantly larger than the vortex-shedding ones and increase with the Reynolds number, and thus with progressively smaller scales. However, it may be concluded that, although these structures are not well resolved in the present simulations, their effects on the bulk quantities of practical interest, such as the aerodynamic loads on the cylinder, are satisfactorily reproduced.

Finally, a sensitivity analysis to the numerical diffusion and the agglomeration level, was carried out at Re=20000. The agglomeration level controls the dimension of the LRS in VMS-LES and, hence, the range of scales on which the SGS model is acting. By increasing the dimension of LRS in each direction, no significant effects were observed on the results. The sensitivity to the value of the parameter controlling the amount of introduced numerical diffusion has also been found to be very low. This is in agreement with the conclusions drawn for the same flow at Re=3900 in [6] and in our previous works [5] for different flows, and confirms that the numerical diffusion introduced by the used numerical scheme does not play a predominant role, also when used in the VMS-LES approach, in which the SGS viscosity is lower than in classical LES and is applied to a limited range of scales.

Acknowledgment

The authors wish to thank Thomas Grinnaert and Marco Bilanceri for their help. CINECA (Italy) is gratefully acknowledged for having provided computational resources and support. Finally, HPC resources from GENCI-[CCRT/CINES/IDRIS] (Grant 2009-c2009025067 and 2009-x2009025044) are also gratefully acknowledged.

References

[1] C. Fureby, Towards the use of large eddy simulation in engineering, *Progress in Aerospace Sciences* 44, 381-396, 2008.

[2] R. Bouffanais, Advances and challenges of applied large-eddy simulation, *Comp. Fluids* 39: 735738, 2010.

[3] P. Tucker and S. Lardeau, Applied large eddy simulation, *Phil. Trans. R. Soc. A*, 367 (1899): 2809-2818, 2009.

[4] S. Camarri, M.V. Salvetti, B. Koobus, and A. Dervieux, Large-eddy simulation of a bluff-body flow on unstructured grids, *Int. J. Num. Meth. Fluids*, 40:1431–1460, 2002.

[5] S. Camarri, M. V. Salvetti, B. Koobus, and A. Dervieux, A low diffusion MUSCL scheme for LES on unstructured grids, *Comp. Fluids*, 33:1101–1129, 2004.

[6] H. Ouvrard, B. Koobus, A. Dervieux, and M.V. Salvetti, Classical and variational multiscale LES of the flow around a circular cylinder on unstructured grids, *Comp. Fluids*, 39:1083–1094, 2010.

[7] T.J.R. Hughes, L. Mazzei, and K.E. Jansen, Large eddy simulation and the variational multiscale method, *Comput. Vis. Sci.*, 3:47–59, 2000.

[8] T.J.R. Hughes and A.A. Oberai and L. Mazzei, Large eddy simulation of turbulent channel flows by the variational multiscale method, *Phys. Fluids*, 13 :1784–1799, 2001.

[9] M. Germano and U. Piomelli and P. Moin and W. Cabot, A dynamic subgrid-scale eddy viscosity model, *Phys. Fluids A*, 3(7): 1760-1765, 1991.

[10] A. Scotti, C. Meneveau, and M. Fatica, Dynamic Smagorinsky model on anisotropic grids, *Physics of Fluids,*, 9(6):1856-1858, 1997.

[11] A. E Tejada-Martinez and K. E. Jansen, A dynamic Smagorinsky model with dynamic determination filter width ratio, *Physics of Fluids*, 16(7):2514-2528, 2004.

[12] C. Meneveau and J. Katz, Scale invariance and turbulence models for large-eddy simulation, *Ann. Rev. Fluid. Mech.*, 32: 1-31, 2000.

[13] B. Koobus and C. Farhat, A variational multiscale method for the large eddy simulation of compressible turbulent flows on unstructured meshes-application to vortex shedding, *Comput. Methods Appl. Mech. Eng.*, 193:1367–1383, 2004.

[14] M.M. Zdravkovich, Flow Around Circular Cylinders. Oxford University Press, 1997.

[15] C.H.K Williamson, Vortex dynamics in the cylinder wake, *Annu. Rev. Fluid.Mech.*, 28, p 477, 1996.

[16] E. Achenbach, Distribution of local pressure and skin friction around a circular cylinder in cross-flow up to $Re = 5 \times 10^6$, *J. Fluid Mech.* 34: 625-639, 1968.

[17] C. Norberg, Fluctuating lift on a circular cylinder: review and new measurements, *J. Fluids Struct.*, 17: 57–96, 2003.

[18] B.J. Cantwell and D. Coles, An experimental study of entrainment and transport in the turbulent near wake of a circular cylinder, *J. Fluid Mech.*, 136, pp. 321-374, 1983.

[19] L. Schiller and W . Linke, Druck- und Reibungswiderstand des Zylinders bei Reynoldsschenzahlen5,000 bis 40,000, *Z. Flugtech. Motorluft*, 24,193 (1933). English translation entitled Pressure and frictional resistance of a cylinder at Reynolds numbers 5,000 to 40,000, in National Ad isoty Committee Aeronautics, Technical Memorandum No. 715, July, 1933.

[20] M.S. Bloor, The transition to turbulence in the wake of a circular cylinder, *J. Fluid Mech.*,,19: 290–304, 1964.

[21] H. Gerrard, A disturbance-sensitive Reynolds number range of flow past a circular cylinder, *J. Fluid Mech.*, 22: 187–, 1965.

[22] A. Prasad and C.H.K. Williamson, The isntability of the shear layer separating from a bluff body, *J. Fluid Mech.*, vol 333, 375–402, 1997.

[23] S. Rajagopalan and R.A. Antonia, Flow around a circular cylinder - srtucture of the near wake shear layer, *Exp. Fluids* 38, 393-402, 2005.

[24] S. Dong and G. E. Karniadakis and A. Ekmekci and D. Rockwell, A Combined DNS-PIV Study of the Turbulent Near Wake, *Journal of Fluid Mechanics*, 569, 185-207, 2006.

[25] C. Chyu and J.-C. Linand and J. Sheridan D. Rockwell, Kàrmàn vortex formation from a cylinder: Role of phase-locked Kelvin-Helmholtz vortices, *Phys. Fluids* 7 (9), 2288-2290, 1995.

[26] J. Ong and L. Wallace, The velocity field of the very near wake of a circular cylinder, *Experiments in Fluids*, vol 20, p 441, 1996.

[27] P. Parnaudeau, J. Carlier, D. Heitz and E. Lamballais, Experimental and numerical studies of the flow over a circular cylinder at Reynolds number 3900, *Phys. Fluids*, 20085101, 2008.

[28] C. Norberg, Effect of Reynolds number and a low-intensity freestream turbulence on the flow around a circular cylinder, Publ. 87/2. Dept. Applied Thermodynamics and Fluid Mechanics, Chalmers University of Technology, 1987.

[29] C. Norberg, Pressure distributions around a circular cylinder in cross-flow, Proceedings of the Symposium on Bluff Body Wakes and Vortex-Induced Vibrations (BBVIV3), Port Arthur, Queensland (Australia), K. Hourigan, T. Leweke, M.C. Thompson and C. H. K. Williamson Eds., 2002.

[30] S. Yokuda and R.R. Ramaprian, The dynamics of flow around a cylinder at subcritical reynolds number, *Phys. Fluids A*, 5:3186–3196, 1990.

[31] R.I. Basu, Aerodynamic forces on structures of circular cross-section. part i: Model-scale data obtained under two-dimensional and low-turbulence streams, *J. Wind Eng. Ind. Aerodynamic*, 21:273–294, 1985.

[32] E. Salvatici and M.V. Salvetti, Large-eddy simulations of the flow around a circular cylinder: effects of grid resolution and subgrid scale modeling, *Wind & Structures*, 6(6):419–436, 2003.

[33] H. Lim and S. Lee, Flow Control of Circular Cylinders with Longitudinal Grooved Surfaces, *AIAA Journal*, Vol. 40, No:10, October 2002.

[34] F. Nicoud and F. Ducros, Subgrid-scale stress modelling based on the square of the velocity gradient tensor, *Flow Turb. Comb.*, 62(3):183–200, 1999.

[35] L. Bricteux, M. Duponcheel and G. Winckelmans, A multiscale subgrid model for both free vortex flows and wall-bounded flows, *Phys. Fluids*, 21, 105102, 2009.

[36] A. Kravchenko and P. Moin, Numerical studies of flow over a circular cylinder at $Re_D = 3900$, *Phys. of Fluids*,12:2, 403-417,2000.

[37] J. Lee, N. Park, S. Lee and H. Choi, A dynamical subgrid-scale eddy viscosity model with a global model coefficient, *Phys. Fluids*, 18:12, 2006.

[38] S. A. Jordan, Investigation of the Cylinder Separated Shear-Layer Physics by Large Eddy Simulation, *International J. Heat Fluid Flow*, 23, 1-12, 2002.

[39] S. Aradag, Unsteady turbulent vortex structure downstream of a three dimensional cylinder, *J. of Thermal Science and Technology* 29(1): 91-98, 2009.

[40] R. Gopalkrishnan, Vortex-induced forces on oscillating bluff cylinders, PhD thesis, Department of Ocean Engineering, MIT, Cambridge, MA, USA. 1993.

[41] M. J. Moeller and P. Leehey, Unsteady forces on a cylinder in cross flow at subcritical Reynolds numbers. In ASME Symposium on Flow-induced Vibrations (ed. M. P. Paidoussis, O. M, Griffin and M. Sevik), New Orleans, ASME, New York, vol. 1, pp. 57–71, 1984.

List of tables:

Table 1: Bulk flow parameters at Re=3900. $\overline{C_d}$ is the mean drag coefficient, C_{Lrms} is the r.m.s. of the time variation of the lift coefficient, l_r is the mean bubble recirculation length, $\overline{Cp_b}$ is the value of the mean pressure coefficient in the rear part of the cylinder, θ_{sep} the mean separation angle, and St the Strouhal number.

Table 2: Bulk flow parameters at Re=10000. The meaning of the symbols is the same as in Tab. 1.

Table 3: Bulk flow parameters at Re=20000. The meaning of the symbols is the same as in Tab. 1.

Table 4: Bulk flow parameters obtained at Re=20000 by varying some simulation parameters. See the caption of Tab. 1 for the meaning of symbols. The percent variation with respect to the reference simulation in Tab. 3 is reported.

Table 1: Bulk flow parameters at Re=3900. $\overline{C_d}$ is the mean drag coefficient, C_{Lrms} is the r.m.s. of the time variation of the lift coefficient, l_r is the mean bubble recirculation length, $\overline{Cp_b}$ is the value of the mean pressure coefficient in the rear part of the cylinder, θ_{sep} the mean separation angle, and St the Strouhal number.

Simulation	$\overline{C_d}$	C_{Lrms}	l_r	-$\overline{Cp_b}$	θ_{sep}	St
Present VMS-LES	0.99	0.108	1.45	0.88	89	.21
VMS-LES [6] (coarser grid)	1.03	0.377	0.94	1.01	–	.22
VMS-LES [6] (finer grid)	0.94	0.092	1.56	0.83	–	.22
LES [27, 36, 37]	[0.99-1.38]	–	[1.0-1.56]	[0.89-1.23]	–	[0.19-0.21]
Experiments [24, 26, 27, 36]	[0.94-1.04]	–	[1.47-1.51]	[0.82-0.93]	–	[0.20-0.22]

Table 2: Bulk flow parameters at Re=10000. The meaning of the symbols is the same as in Tab. 1.

Simulation	$\overline{C_d}$	C_{Lrms}	l_r	-$\overline{Cp_b}$	θ_{sep}	St
VMS-LES WALE	1.22	0.476	0.87	1.15	87	0.20
DNS [24]	[1.11-1.21]	[0.45-0.57]	0.82	[1.06-1.20]	–	[0.19-0.21]
Experiments [24, 28, 17, 40, 41]	1.19	[0.38-0.53]	0.78	1.11	–	[0.19-0.20]

Table 3: Bulk flow parameters at Re=20000. The meaning of the symbols is the same as in Tab. 1.

Simulation	$\overline{C_d}$	C_{Lrms}	l_r	-$\overline{Cp_b}$	θ_{sep}	St
VMS-LES WALE	1.27	0.60	0.80	1.09	86	0.19
LES [39]	–	–	1.	[1.04-1.25]	–	–
LES [32]	[0.94-1.28]	[0.17-0.65]	[0.7-1.4]	[0.83-1.38]	–	–
Experiments [17, 33, 30, 31]	[1.10-1.20]	[0.4-0.6]	–	[1.03-1.09]	–	0.194

Table 4: Bulk flow parameters obtained at Re=20000 by varying some simulation parameters. See the caption of Tab. 1 for the meaning of symbols. The percent variation with respect to the reference simulation in Tab. 3 is reported.

Simulation	γ	cell agglom.	$\Delta\overline{C_d}$	Δl_r	ΔSt	-$\Delta\overline{Cp_b}$
VMS-LES WALE	0.2	1 level	+2.2 %	<1%	-1.5 %	+3.7%
VMS-LES WALE	0.3	2 levels	+1.5%	+1.5%	+ 1%	+2.2%

List of figures:

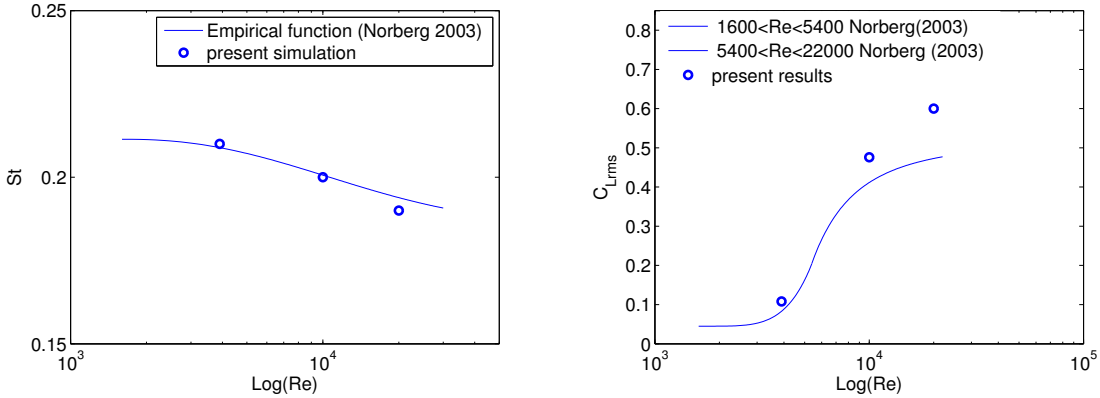

(a) (b)

Figure 1: Comparison of the present results with the empirical functions proposed in [17]; (a) Strouhal number; (b) r.m.s. of the lift coefficient.

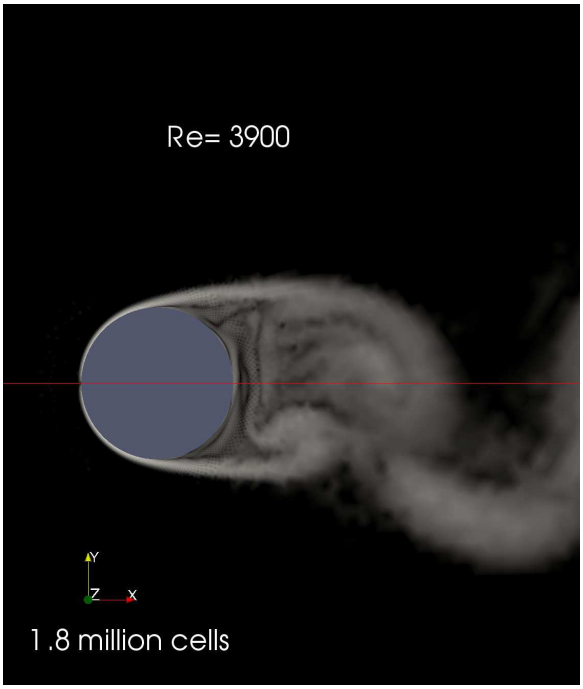

Figure 2: Snapshot of vorticity modulus at Re=3900.

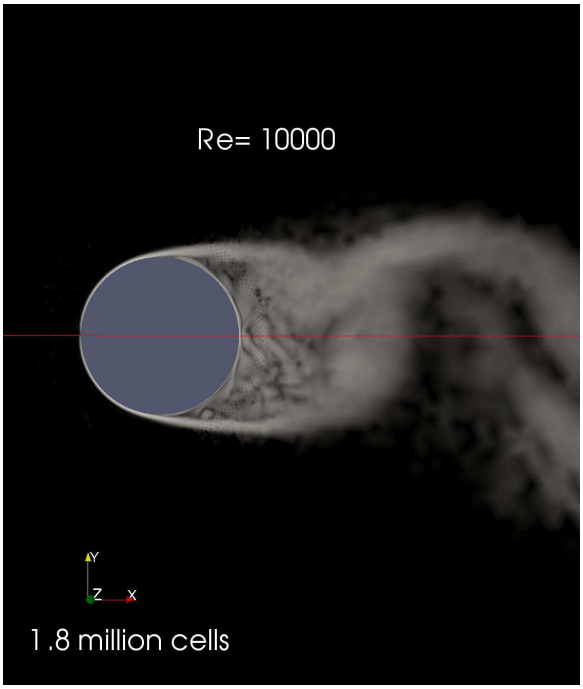

Figure 3: Snapshot of vorticity modulus at Re=10000.

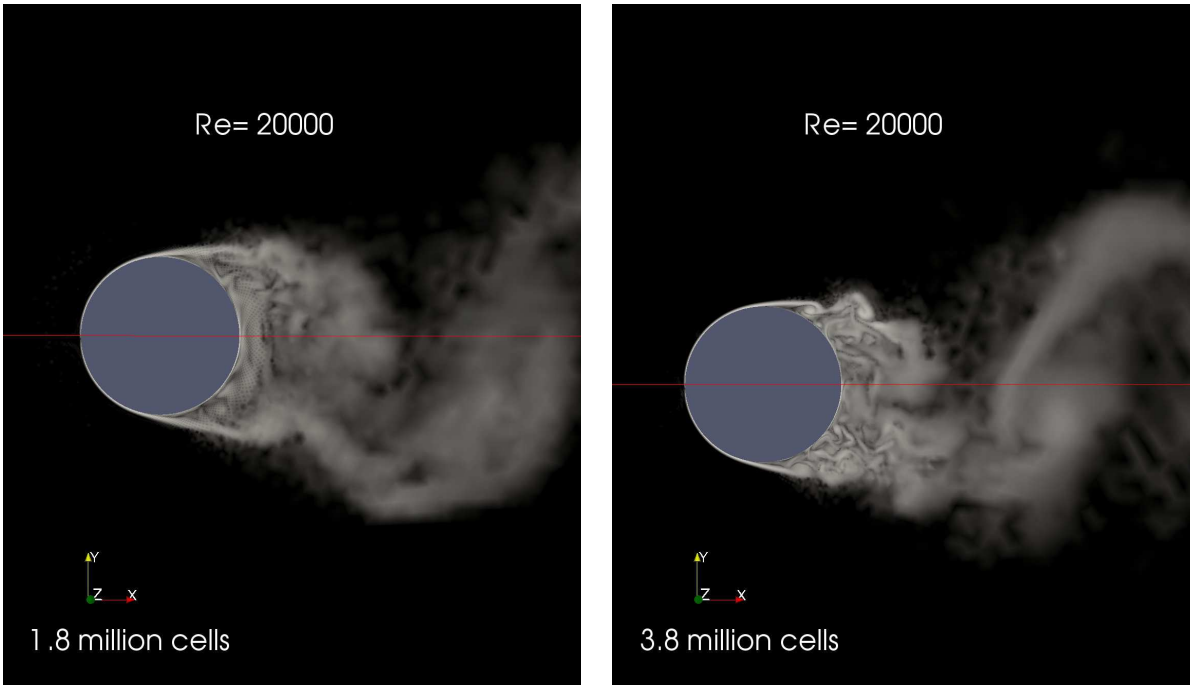

(a) (b)

Figure 4: Snapshot of vorticity modulus at Re=20000. (a) coarse grid; (b) refined grid.

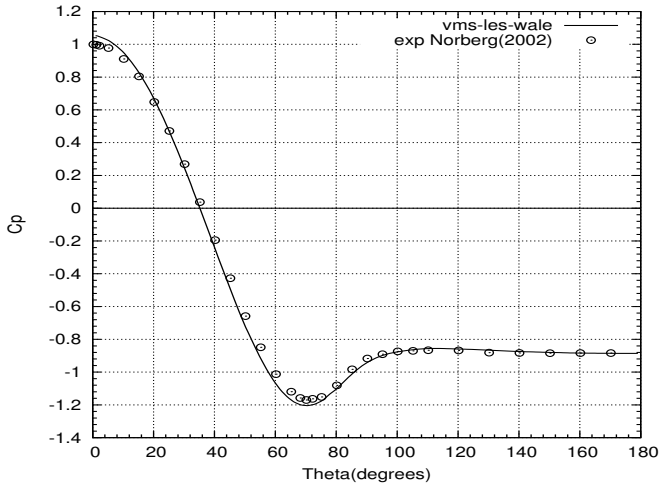

Figure 5: Mean pressure coefficient distribution at the cylinder at Re=3900.

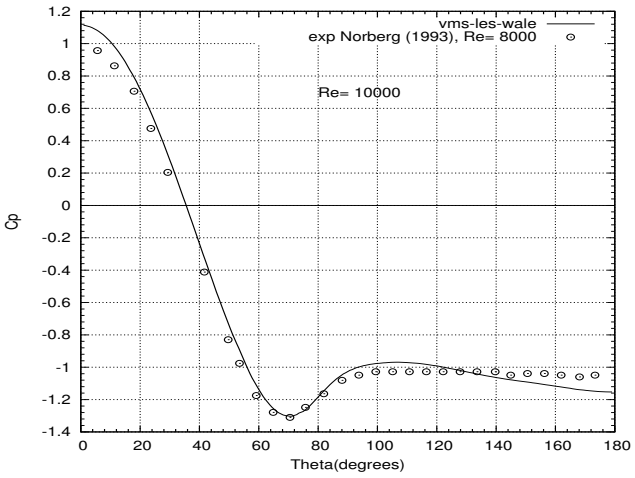

Figure 6: Mean pressure coefficient distribution at the cylinder at Re=10000.

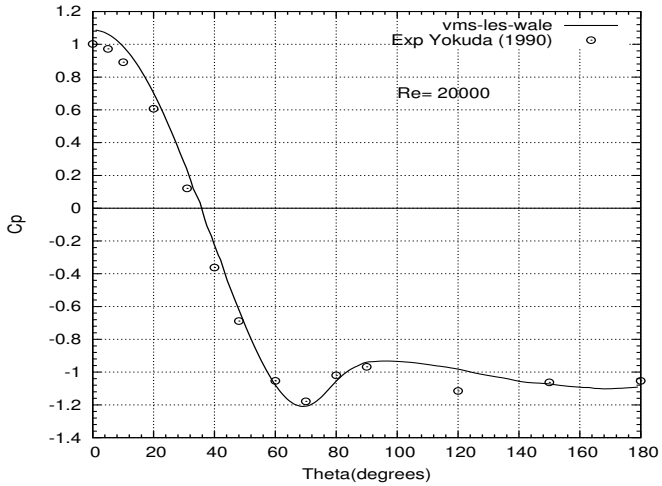

Figure 7: Mean pressure coefficient distribution at the cylinder at Re=20000.